JOURNAL OF CATALYSIS **166,** 53–66 (1997)
ARTICLE NO. CA971503

Gas Phase Synthesis of MTBE from Methanol and Isobutene over Dealuminated Zeolites

F. Collignon, M. Mariani, S. Moreno, M. Remy, and G. Poncelet[1]

Unité de Catalyse, Université Catholique de Louvain Place Croix du Sud 2/17, B-1348 Louvain-la-Neuve, Belgium

Received July 22, 1996; revised October 21, 1996; accepted October 28, 1996

Gas phase synthesis of MTBE from methanol and isobutene has been investigated over different zeolites. It is shown that bulk Si/Al ratio has a marked influence on the formation of MTBE. H-beta zeolite was found to be as active as acid Amberlyst-15 (reference catalyst), and noticeably superior to non- and dealuminated forms of H-Y, H-ZSM-5, zeolite omega, and H-mordenites. Screening test results obtained over other catalysts (SAPOs and pillared clays) are briefly commented. The contribution of the external surface of the zeolites to the reaction is discussed. In the case of H-Y zeolites, it is shown that extraframework Al species (^{27}Al NMR signal at 30 ppm) have a detrimental effect on the reaction.

INTRODUCTION

MTBE (methyl tertiary-butyl ether) is the most largely used quality-improving additive for unleaded gasolines. As other ethers, it easily mixes with gasoline, has excellent antiknocking behavior and reduced emission of pollutants, but its production cost is lower than for other ethers (1). Worldwide production of MTBE has increased faster than for most other commodity chemicals (2) with, in 1994, a total capacity of about 18.5×10^6 tons and an estimated increasing yearly demand of 15% for the next coming years (3). Decomposition of the ether is as well of industrial interest because it is a route to pure isobutene.

The industrial production of MTBE is carried out in liquid phase over sulfonic acid resins (e.g., Amberlyst-15) at temperatures of the order of 50–70°C, pressures between 10 and 15 bar, and methanol (MeOH)/isobutene (IB) molar ratios higher than 1:1 (4). The reaction is exothermic and requires careful control of temperature. Diisobutenes (2-4-4 trimethyl-1- and 2-pentenes), tertio-butyl alcohol, and dimethylether are the main side products, but other possible ones have been mentioned (5). Sulfonic acid resins are quite performing catalysts with, however, some limitations such as thermal fragility of the sulfonic groups (generating corrosion problems (6)), and use of relatively high methanol/isobutene molar ratios which requires recycle operations. Alternative catalysts exempt from the drawbacks of the sulfonic resins have been investigated, principally zeolites and, to a lesser extent, heteropoly acids (7, 8), layered Zr- and Ti-phosphates (9), and sulfate-modified zirconia/ZSM-5 composite system (10). Silica-supported tantalum oxide has been shown to be an efficient catalyst for the reverse reaction (11).

Several studies have been devoted, in recent years, to the gas phase synthesis of MTBE from MeOH and IB, or from methanol and isobutanol (12), and ETBE from EtOH and IB (13) over protonated zeolites. Chu *et al.* (14) and Nikolopoulos *et al.* (15) showed that zeolites were less active than Amberlyst-15, but more selective to MTBE, in particular H-ZSM-5 (less deactivation). Ti-silicalite appeared to be even more selective than H-ZSM-5 (16). Kogelbauer *et al.* (17, 18) observed in the case of dealuminated H-Y zeolites, a strong increase of the TOF as the concentration of the acid sites was reduced, which they attributed to interaction between extra-lattice Al and Brønsted acid sites. Impregnation with triflic acid (TFA), a strong electron withdrawer, was shown to enhance, up to a given threshold, the activity of H-Y zeolite (not observed for H-ZSM-5), without reaching, however, the performance of acid resins (17, 19, 20). According to the authors, the enhancement of activity was apparently related to the formation of extra-lattice Al by the TFA modification rather than to the presence of TFA. Recently, Nikolopoulos *et al.* (21) observed over H-Y, H-mordenite, and H-ZSM-5 modified by ion-exchange with ammonium fluoride a similar beneficial effect on the reaction rate with increasing F^-/Al ratio. As for the zeolites treated with triflic acid, the enhanced activity was attributed to extraframework Al species produced by the fluoride treatment. Improved activity was also observed upon addition of ammonium sulfate (22), whereas partial cation-exchange of zeolites H-Y did not result in an increased activity (17, 23). MeOH being preferentially adsorbed over IB, preadsorption of MeOH prior to IB introduction increased the rate of formation of MTBE (24).

[1] Author for correspondence.

0021-9517/97 $25.00

As most acid zeolites are thermally stable, they should constitute suitable catalysts, in particular, for integrated processes from syngas to methanol to MTBE (18). This work aims to compare the results of screening experiments of gas phase synthesis of MTBE from isobutene and methanol carried out over different types of dealuminated zeolites, pillared clays, and a sulfonic acid resin (Amberlyst-15) taken as a reference catalyst.

EXPERIMENTAL

Catalysts

Several catalysts were considered in this screening study. Most were acid forms of zeolites, namely large- and small-port mordenites, ZSM-5, zeolite Y, zeolite omega, zeolite beta, and SAPOs. Other catalysts such as Zr- and Al-pillared clays also have been evaluated. The reference catalyst was Amberlyst-15 (sulfonic acid resin from Aldrich). The different catalysts are presented in Table 1.

The series of ZSM-5 and zeolites Y, and the starting zeolite beta were supplied by PQ Zeolite; SAPOs and zeolite omega were UOP samples; starting mordenites were from Société Grande Paroisse, France (small-port variety, SP), and Tosho Corp., Japan (large-port variety, LP).

The two varieties of mordenites were dealuminated either by steaming treatments and subsequent acid leaching with 6 *M* HNO_3 at reflux to remove extraframework Al species (samples STH; f. i. S600H, standing for steaming at 600°C followed by acid leaching) or by calcination, acid leaching (6 *M* HNO_3) and second calcination at the same temperature (samples THT; f. i. 500H500 standing for calcination at 500°C, acid leaching with 6 *M* HNO_3, and second calcination at 500°C). Dealumination by acid attack alone (f. i., H 9h meaning acid attack with 6 *M* HNO_3 at reflux for 9 h) or in combination with steam treatment (f. i. H 24h S600H meaning acid attack with 6 *M* HNO_3 for 24 h at reflux followed by steaming at 600°C for 3 h and subsequent acid leaching with 6 *M* HNO_3 at reflux for 3 h) was also performed (25). Dealumination of zeolite beta (ZB-25, P.Q.) was carried out according to a procedure described in the literature (26). Briefly, 1 g zeolite was added into 200 ml of HNO_3 solution previously heated at 80°C, and the mixture was stirred for 3 h at this temperature. Acid concentrations between 0.02 and 3.8 *M* were used (see Table 1). The solids were hot-filtered and washed with demineralized water until the conductivity of the residual water was reduced to its initial value and dried at 100°C for 1 h.

Dealumination of zeolite omega (LZ6) was done by steaming at different temperatures between 600 and 750°C followed by acid leaching under reflux for 4 h with either 0.24 or 1.22 *M* HNO_3. This procedure is similar to the one reported by Jaquinot *et al.* (27) and Ponthieu *et al.* (28).

TABLE 1

Si/Al Bulk Ratio, Relative Crystallinity (%), External Surface Area ($m^2 \cdot g^{-1}$), and Micropore Volume ($cm^3 \cdot g^{-1}$)

Sample	Si/Al	Rel.cryst.	Sext [a]	V μ [a]
Zeolite Beta				
ZB25	13.2	100.0	218.8	0.23
0.02 N	20.6	104.4	221.7	0.21
0.03 N	n.d.	98.4	n.d.	n.d.
0.04 N	20.6	91.0	221.4	0.21
0.05 N	25.7	84.9	211.4	0.22
0.06 N	28.4	85.7	229.4	0.22
0.08 N	n.d.	92.4	235.2	0.22
0.11 N	46.3	83.1	234.3	0.21
0.25 N	94.5	76.1	219.9	0.20
0.5 N	94.5	69.5	n.d.	n.d.
1.0 N	n.d.	83.5	240.5	0.18
1.6 N	92.6	74.7	n.d.	n.d.
3.8 N	194.2	79.1	n.d.	n.d.
Zeolite Y				
CBV 500	2.6	100.0	55.3	0.27
CBV 600	2.8	91.0	51.2	0.24
CBV 712	5.8	121.0	109.5	0.25
CBV 720	13.0	127.0	103.3	0.27
CBV 740	21.0	105.0	150.6	0.32
CBV 760	30.0	40.0	143.2	0.25
CBV 780	37.0	89.0	112.4	0.27
ZSM-5				
CBV 3020	16.5	76.5	106.5	0.14
CBV 5020	25.0	81.8	111.6	0.14
CBV 8020	38.3	78.5	162.8	0.12
CBV 1502	77.5	79.8	n.d.	n.d.
CBV 3002	123.5	100.0	n.d.	n.d.
CBV 2802	137.5	96.6	n.d.	n.d.
S.P. mordenites				
ZM 101	5.8	100.0	9.4	0.19
H3h	7.7	82.1	16.0	0.19
H24h	11.4	88.3	39.0	0.18
550H550	13.0	83.5	46.0	0.20
600H600	39.2	87.6	47.0	0.20
S500 H	74.1	94.4	41.0	0.20
S600 H	99.0	96.7	59.0	0.20
S700 H	120.6	98.0	85.0	0.19
H24h S600 H	111.5	91.6	106.0	0.19
L.P. mordenites				
HSZ 600	8.1	100.0	25.7	0.19
H 9h	53.2	83.0	58.0	0.19
550H550	74.0	92.5	75.0	0.21
700H700	127.6	89.0	92.0	0.21
S600 H	96.8	93.1	87.0	0.20
S600 H1	35.0	78.1	68.0	0.22
S700 H	194.7	88.7	80.0	0.21
H 24h S600 H	111.5	90.5	80.0	0.18
Zeolite omega				
LZ6	4.2	100	n.d.	n.d.
S700 H 0.24	4.7	60	n.d.	n.d.
S600 H 0.24	4.8	75	n.d.	n.d.
S650 H 0.24	4.9	62	n.d.	n.d.
S600 H 1.22	5.5	74	n.d.	n.d.
S700 H 1.22	23.1	49	n.d.	n.d.
S650 H 1.22	25.8	26	n.d.	n.d.
S675 H 1.22	26.4	36	n.d.	n.d.
S750 H 1.47	29.3	35	n.d.	n.d.
S675 H 2.45	52.4	31	n.d.	n.d.
S750 H 1.22	n.d.	34	n.d.	n.d.
Pillared clays				
Zr-P-M	n.d.	n.d.	n.d.	n.d.
Al-P-S	n.d.	n.d.	n.d.	n.d.

a, calculated according to Ref. (32).
n.d., not determined.

The series of H-Y and H-ZSM-5 were used as received (no further dealumination). Samples CBV-500 and -712 supplied in the ammonium form were previously converted in the protonic forms by a calcination step at 500°C for 14 h under air stream.

The Al- and Zr-pillared materials (AlP-S and ZrP-M) were prepared as described elsewhere (29, 30). S and M refer to the type of smectite, namely saponite (S) and montmorillonite (M).

Reference Amberlyst-15 was previously treated following the procedure recommended by Volosch *et al.* (31) and adopted by several authors. Pretreatment was done at 90°C for 3 h under a stream of helium.

Characterisation

The relative crystallinities of the dealuminated samples were established from X-ray diffraction recordings obtained with a Siemens D-5000 diffractometer and copper anticathode. The relative crystallinities were evaluated by the ratio of the sum of the areas of the main peaks to the sum of the values obtained for the starting zeolite. In the case of ZSM-5, sample CBV-3002 exhibited higher peak intensities (and areas) among the series and, therefore, was taken as reference.

The bulk Si/Al ratios were established from the Al contents determined by inductively coupled plasma spectroscopy (ICPS).

The textural characteristics (external surface areas and micropore volumes) were obtained from nitrogen adsorption isotherms, using the approach proposed by Remy *et al.* (32).

Catalytic Measurements

The reaction was carried out in gas phase in a fixed bed U-shaped glass reactor operated at atmospheric pressure, using methanol (MeOH)/isobutene (IB) molar ratio of 1.02, and a WHSV of 3.25 h^{-1}. Methanol vapor was generated by passing a stream of helium ($5{,}77 \times 10^{-4}$ mol min^{-1}) through a glass saturator thermostated at 25°C. Flows were monitored by mass flow controllers. The reaction was studied at temperatures between 30 and 120°C, and a heating rate of 0.3°C min^{-1}. A thermocouple was placed near the catalytic bed to achieve continuous monitoring of temperature. All tubings, valves, and connections in front of the reactor were heated at 60°C, and at 120°C between the outlet of the reactor and the gas chromatograph. Before the catalytic evaluation, in-situ activation of the catalyst was done at 400°C for 3 h under a stream of helium. On-line gas phase analysis was done in a H.P.-5890 gas chromatograph equipped with TC-type detector and 30-m capillary column (cross-linked methyl silicone from H.P.). Sampling of the gaseous effluent was monitored every 16.67 min by means of an automated 6-way sampling valve.

Yields, conversions, and selectivities were calculated by taking into account the number of moles of reacted and unreacted isobutene. It was controlled that the conversions were proportional to the catalyst weight.

RESULTS

The values of the bulk Si/Al ratios, relative crystallinities, external surface areas (Sext), and micropore volumes of the series of dealuminated zeolites are given in Table 1. As mentioned in the experimental section, the series of zeolite Y and ZSM-5 were used as received (no further dealumination). Except for the samples of zeolite omega, the crystallinities of the dealuminated forms are generally well preserved. For the series of zeolite omega, important losses of crystallinity are noticed (reason why the textural characteristics have not been established). In first analysis, the micropore volumes are little modified by the dealumination treatment. Large- and small-port mordenites, and zeolites beta have similar micropore volumes. Sext generally increases with increasing Si/Al ratio and zeolite beta exhibits rather large external surface areas compared with the other zeolites.

The curves showing the variation of the yield of MTBE versus reaction temperature are presented in Figs. 1 to 6 for the different zeolites investigated. All the curves exhibit similar "volcano" type profiles, namely increasing yields of MTBE as temperature increases, reaching of a maximum, and decreasing yields beyond this maximum. Generally, the experimental values of the decreasing part of the curves align on a same curve which corresponds to the thermodynamic equilibrium of the reaction at the corresponding temperature. A representation of the thermodynamic curve, established from the data of Tejero *et al.* (33), is shown in Fig. 1. It shows that in gas phase conditions, the most active catalysts are those which operate the reaction at lower temperatures.

The results obtained over the series of commercial zeolites H-Y (Fig. 1) show that the least dealuminated samples, with bulk Si/Al ratio of 2.6 (CBV500) and 2.8 (CBV600), are the least active ones among the series. Sample with bulk Si/Al ratio of 30 (CBV760) is the most active one, and those with intermediate ratios (CBV712, -720, and -740) or with Si/Al ratio greater than 30 (CBV 780) exhibit intermediate activities.

Figure 2 refers to the catalytic results obtained over H-ZSM-5 zeolites, in which the Si/Al ratios spread over a broader range. The most active one (CBV5020) has a bulk Si/Al ratio of 25, namely close to one of the best sample of the series of zeolites H-Y. Samples with slightly lower (16.5 for CBV3020) or slightly higher Si/Al ratios (38.2 for CBV8020) have comparable activities. Sample with Si/Al ratio of 78.5 (CBV1502) reaches the same yield of MTBE at maximum conversion as the two latter ones, but the maximum occurs at a higher temperature. Note also that the maximum yield of MTBE over the best sample of the H-ZSM-5 series is slighlty lower than over the most active sample of the series of H-Y zeolites (27 vs 29 %). It is also observed that up to about 65°C, higher amounts of MTBE

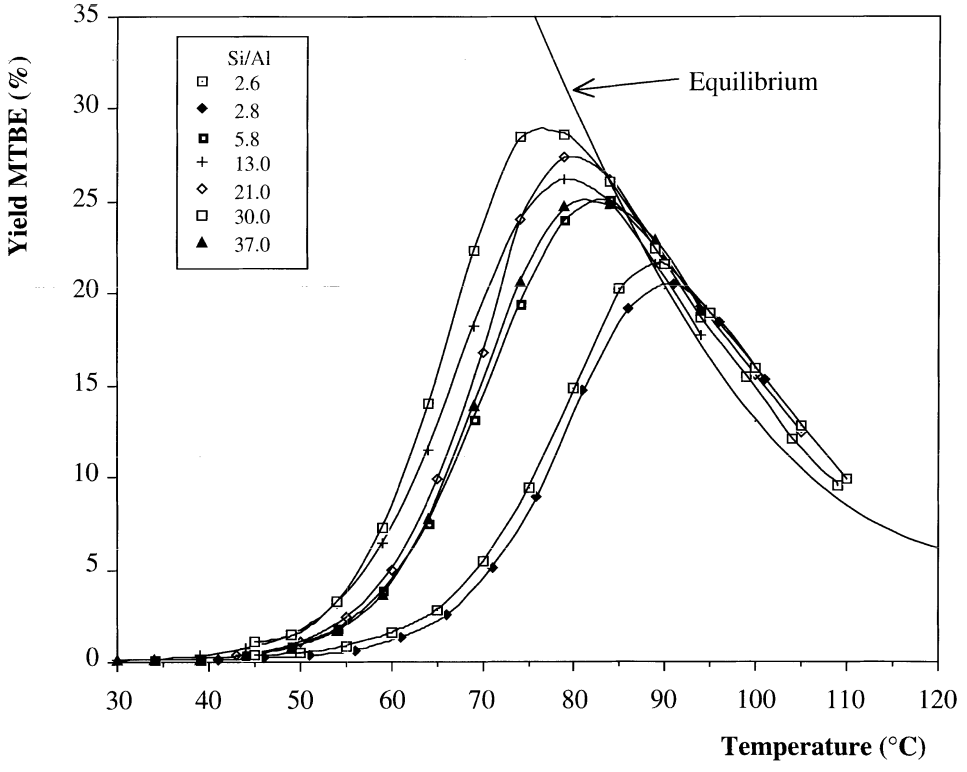

FIG. 1. Zeolites H-Y: yield of MTBE vs reaction temperature and equilibrium curve.

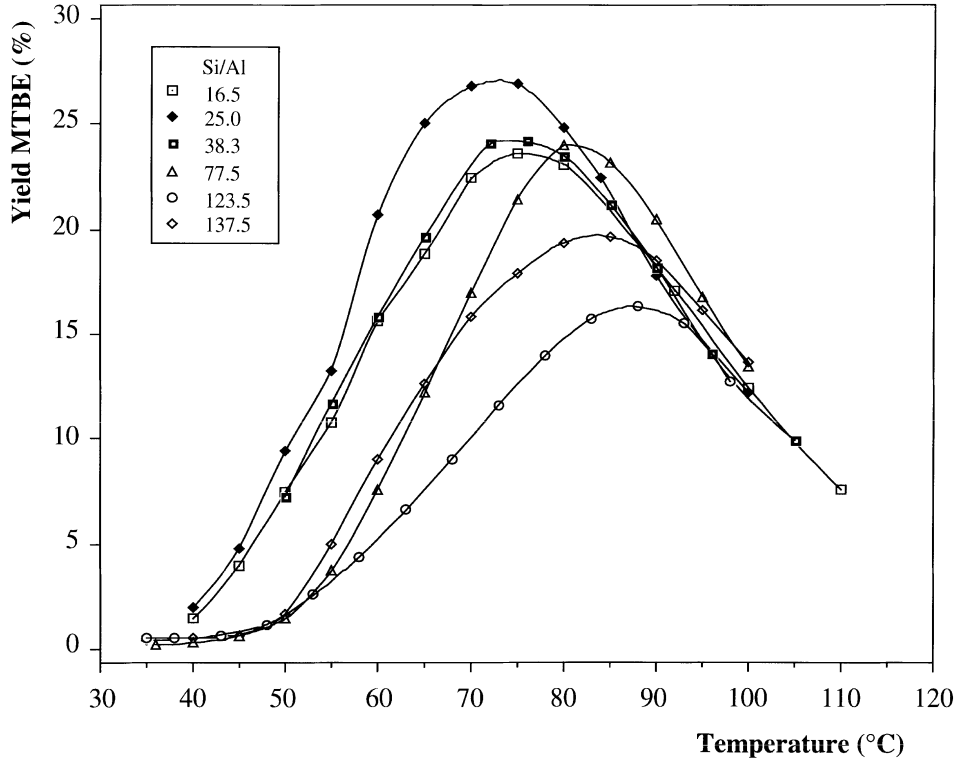

FIG. 2. H-ZSM-5: yield of MTBE vs reaction temperature.

are produced over the three most active H-ZSM-5 zeolites compared with the most active samples of the series of H-Y zeolites.

The conversion curves obtained over the starting and dealuminated forms of large- and small-port mordenites are shown in Figs. 3 and 4.

Among the different samples of large-port mordenites (Fig. 3), which have bulk Si/Al ratios between 8.1 (starting zeolite) and 195, the most active sample has a ratio of 35, and the least active ones are the initial sample and those dealuminated by direct acid attack (sample 24h, with Si/Al ratio of 53) or acid treatment combined with steaming at 600°C and acid leaching (sample H24h-S600H, with Si/Al of 111.5). Next to the most active sample are two dealuminated samples with Si/Al ratios of 74 and 96.8 for which the conversion curves are superimposed. Then, in decreasing order of activity, are samples with Si/Al ratios of 127.6 and, with similar conversion curves, dealuminated samples with ratios of 53 and 194.7.

The results obtained over a series of dealuminated small-port mordenites are shown in Fig. 4. In this series, the Si/Al ratios ranged between 5.8 (starting sample) and 121. Three samples are markedly less active than the others, namely those with the lowest Si/Al ratios (respectively, in increasing order of conversion, 7.7, 11.4, and 5.8). For the samples with Si/Al ratios between 39 and 121, the amplitude of variation at maximum yield of MTBE is significantly reduced in comparison with the series of large-port mordenites.

The results obtained over the series of zeolite omega are shown in Fig. 5. The nondealuminated sample exhibits a poor conversion. For the dealuminated samples, two sets of curves may be distinguished according to the Si/Al ratios, the most active ones having higher dealumination degrees (Si/Al ratios greater than 20). It should be noted that the most active samples are those which exhibit the most important losses of crystallinity.

The best catalytic performances were observed over the series of zeolites H-beta, as shown in Fig. 6. Indeed, under identical reaction conditions, the yields of MTBE produced at maximum conversion are comparable with those obtained over the reference acid resin. Also, even the least active sample among the beta zeolites is more active than the most active sample of the H-Y zeolites. This figure also illustrates the high sensitiveness of the catalytic performances to the dealumination treatment, namely the concentration of the acid solution. A deactivation test has been carried out on sample ZB25 at maximum conversion to MTBE. After 72 h time on stream no loss of activity could be observed.

In order to summarise the catalytic results of Figs. 1 to 6, the yields of MTBE taken at maximum conversion reported to the value obtained over Amberlyst-15 have been plotted, in Fig. 7, in regard to the type of zeolite. The results obtained over SAPO-5, and Al- and Zr-pillared clays tested

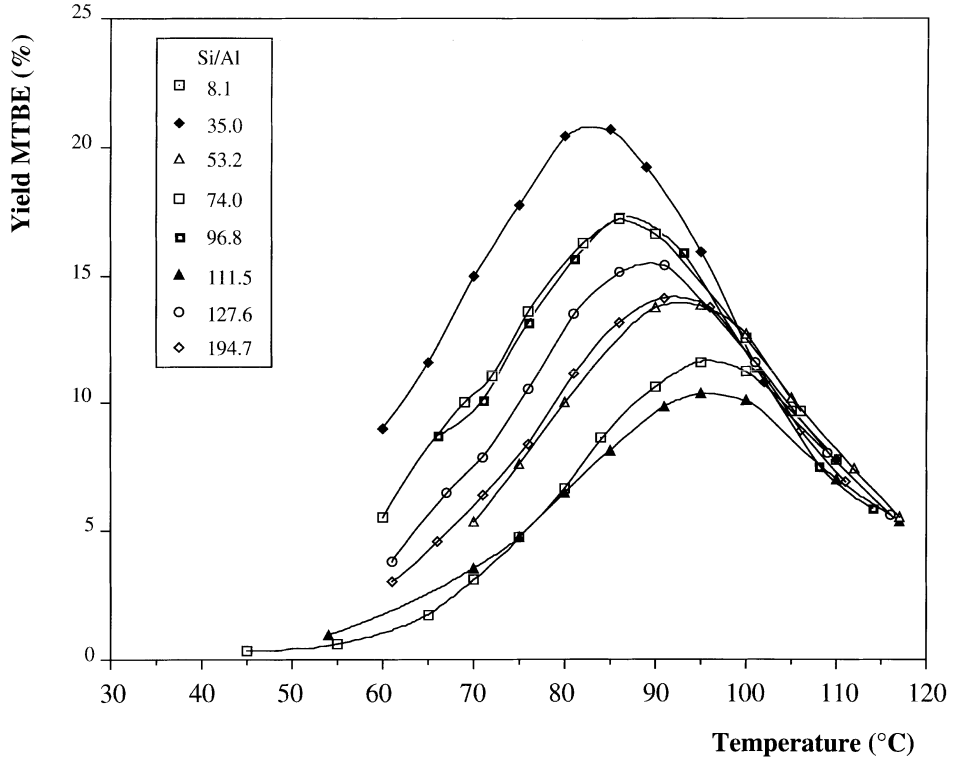

FIG. 3. Large-port mordenites: yield of MTBE vs reaction temperature.

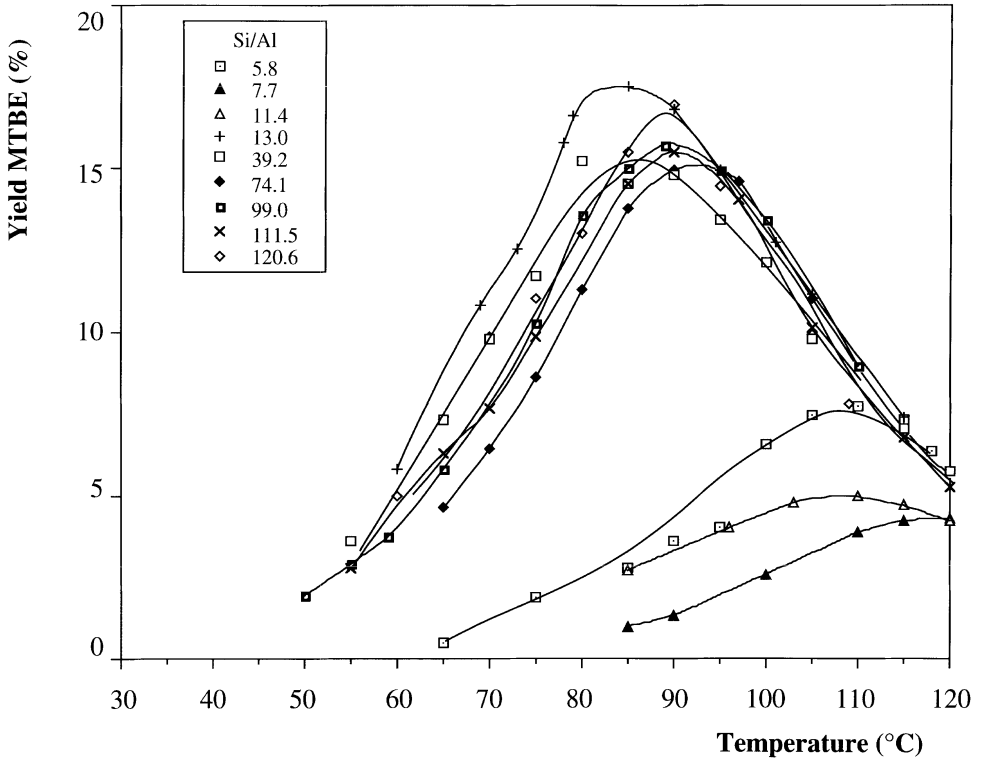

FIG. 4. Small-port mordenites: yield of MTBE vs reaction temperature.

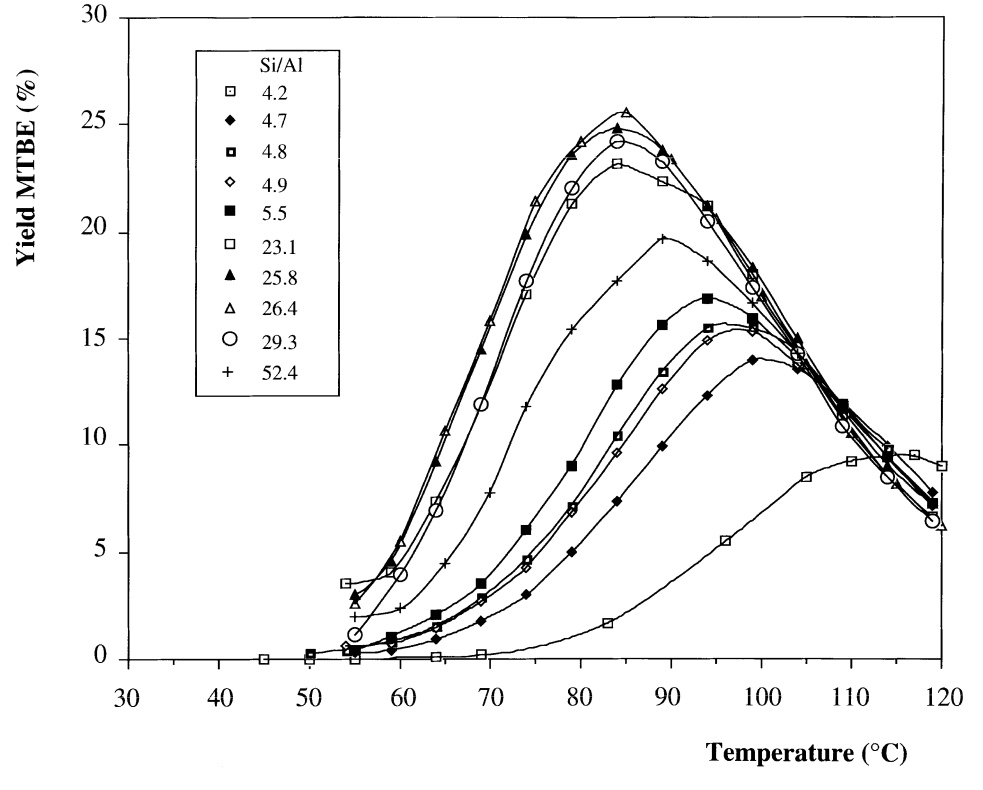

FIG. 5. Zeolites omega: yield of MTBE vs reaction temperature.

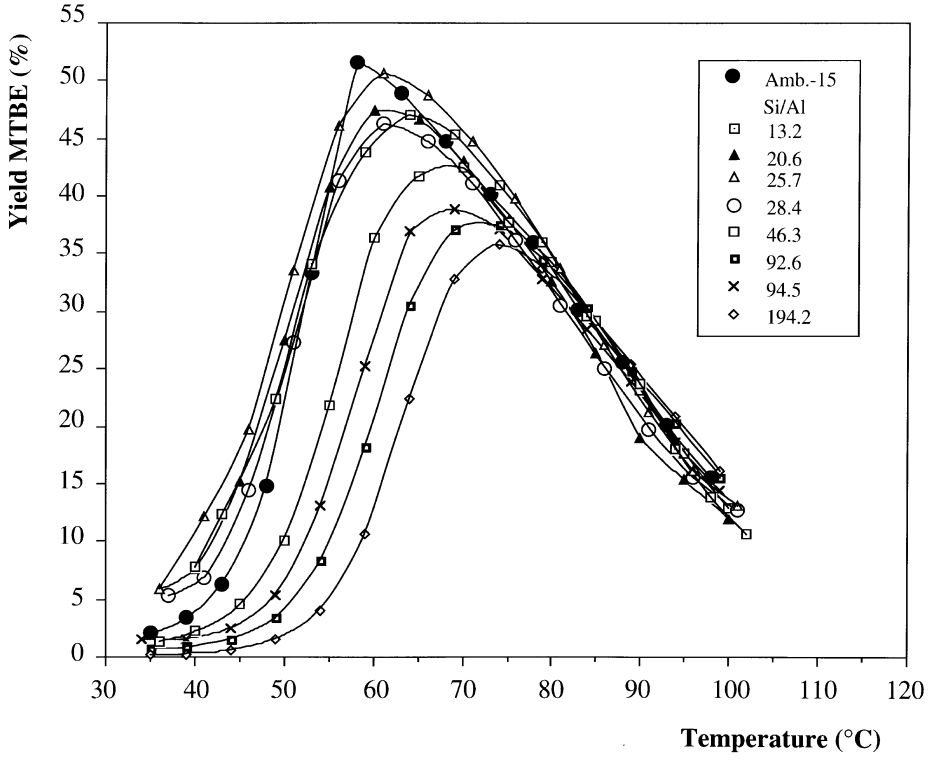

FIG. 6. Zeolites beta and Amberlyst-15: yield of MTBE vs reaction temperature.

under identical conditions have been included. SAPO-11, -34, and -31 were as well tested, but because of their low activities, respectively, 7, 5, and 3% MTBE at maximum IB conversion, they have not been included in the figure. The higher efficiency of the zeolites beta with respect to the other catalysts tested is evident. Three zeolites show nearly identical performances: H-Y, omega, and ZSM-5. Interestingly, Zr-pillared montmorillonite was found as active as the most active H-Y and, surprisingly, superior to Al-pillared saponite.

So far, the formation of side products, in particular diisobutenes (DIB) and dimethylether (DME), has not been addressed. As the DIB's have a high octane number, their admixture to MTBE does not constitute, per se, a major problem, except that these dimers may lead to the formation of heavier products which have a detrimental action on

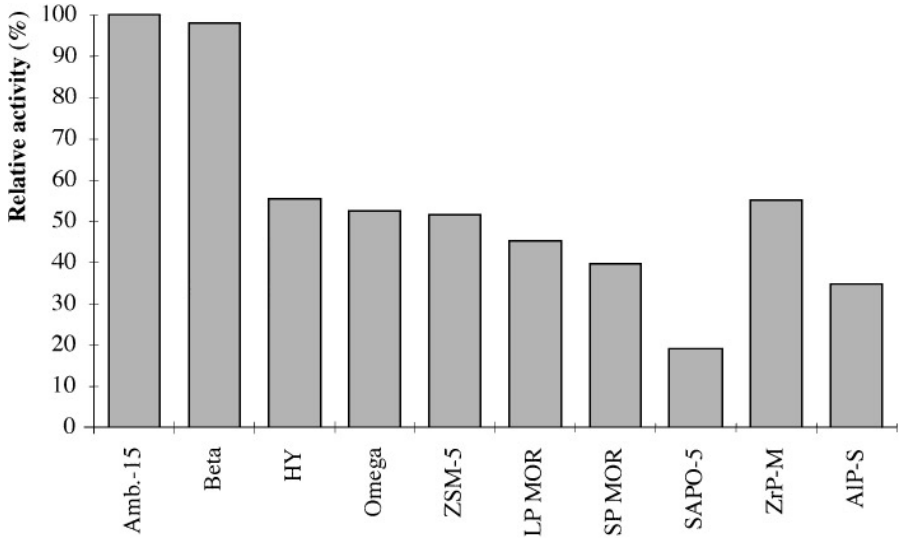

FIG. 7. Relative yields of MTBE at maximum conversion for the different catalysts.

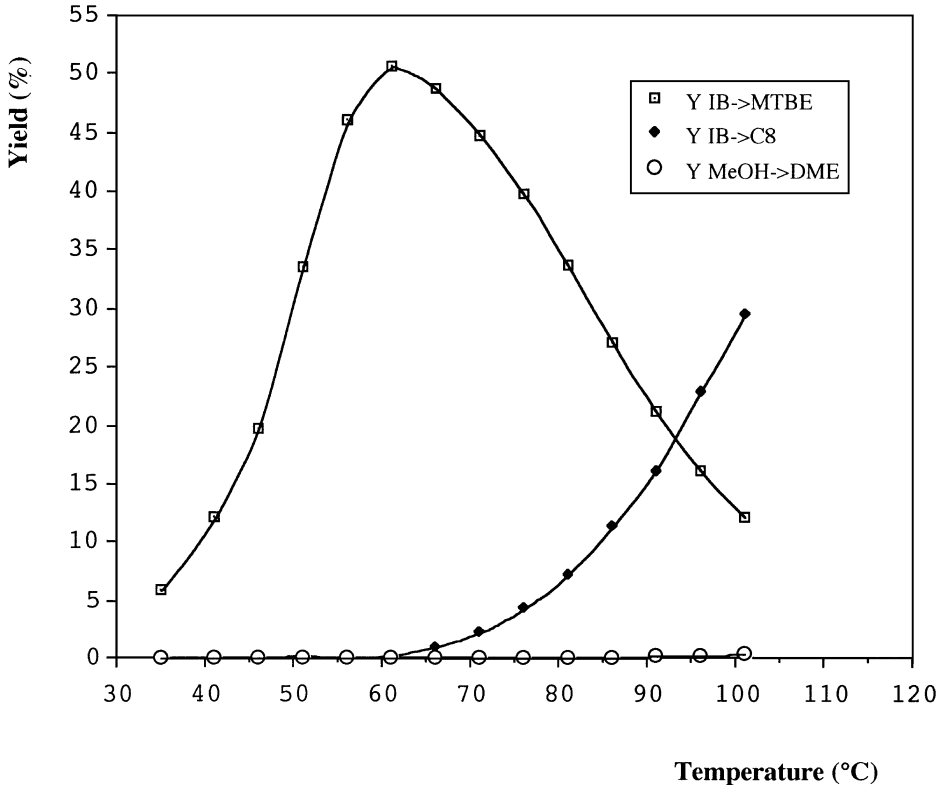

FIG. 8. Conversion of isobutene (IB) into MTBE and diisobutenes (DIB), and of methanol into dimethylether (DME) vs reaction temperature over zeolite beta (sample ZB25 0.05).

the catalyst life (5). Over most of the zeolites investigated (H-Y, H-ZSM-5, omega, beta) as well as over the acid resin, dimerisation of isobutene was inexistant or rather limited up to the temperature of maximum conversion of IB into MTBE. The selectivities to the ether, indeed, were included between 97 and 100%. Beyond this maximum, namely as temperature increased, thermodynamics imposed the reverse reaction: total conversion of isobutene (and yield of MTBE) decreased and, simultaneously, dimerisation of isobutene took over, to become, with further increase of temperature, the main reaction, with rates depending on type of zeolite and Si/Al ratio. On the contrary, over mordenites and SAPOs, DIB started to appear well before the maximum MTBE was reached. With respect to C8 formation, zeolites beta, the most active zeolites toward ether formation, also produced higher amounts of C8 (higher also than over the resin), as it could be presumed. The average proportions of C8 (selectivities) among the reaction products observed at 94°C were as follows:

H-ZSM-5 series: 1.7% (with extremes between 0 and 10%)
H-Y series: 7.4% (between 0 and 14.8%)
H-omega series: 3.5% (between 0.2 and 6.5%)
H-LP mordenites: 23% (between 13 and 29.5%)
H-SP mordenites: 20.5% (between 15.1 and 27.8%)
H-beta series: 41.8% (between 25.3 and 52.5%)
Amberlyst-15: 37%.

Concerning dimethylether (DME), its occurrence in the temperature domain investigated was always restricted to very low amounts (less than 1% of methanol transformed) in the ascending part of the curves shown in Figs. 1 to 6, except for mordenites (as mentioned earlier) and SAPOs. Over most zeolites, the formation of DME started after dimerisation reaction of IB, namely near the higher temperatures investigated, as illustrated in Fig. 8 for H-beta 25 (0.05 *M*).

Activation Energy

The values of the apparent activation energies determined from Arrhenius' plots (ln rate vs T^{-1}) are compiled in Table 2 regarding the temperature domain in which there were established. They were obtained from at least four experimental measurements, imposing a regression coefficient of 0.99 and higher. Significant differences are observed within each series of zeolites (less marked for H-Y zeolites), and between the different zeolites. The average values (in kJ/mol) are as follows: 127 for the series of H-Y; 119 for the beta zeolites; 113 for the series of omega zeolites; 104 for the samples of H-ZSM-5; 61 for the large-port mordenites, 58 for the small-port mordenites, and 171 kJ for the

TABLE 2

Maximum Yield of MTBE, Ymax (% mol.), Rate of MTBE Synthesis at 60°C (μmol · g^{-1} · s^{-1}), Turnover Frequency at 60°C, TOF (10^3 s^{-1}), Logarithm of the Preexponential Term of Arrhenius Equation and Apparent Activation Energy (kJ · mol^{-1})

Sample	Ymax	rate 60°C	TOF[a]	ln(ko app.)	Ea app.	T range
Zeolite Beta						
ZB25	47.0	4.9	4.6	22.0	93.7	40->53
ZB25 0.02 N	47.4	5.4	5.4	21.1	91.1	36->55
ZB25 0.03 N	46.9	5.1	5.2	25.6	102.5	41->51
ZB25 0.04 N	46.6	5.1	5.9	19.2	85.4	36->50
ZB25 0.05 N	50.6	5.4	6.5	20.6	89.4	35->46
ZB25 0.06 N	46.2	5.0	7.5	30.5	116.4	41->51
ZB25 0.08 N	46.0	4.9	9.6	29.7	114.8	40->50
ZB25 0.11 N	42.5	4.0	8.6	35.1	131.3	40->55
ZB25 0.25 N	41.2	3.4	14.2	33.3	127.0	40->60
ZB25 0.5 N	38.9	3.0	15.3	32.0	123.8	39->59
ZB25 1.0 N	38.9	2.7	11.9	41.1	149.4	45->60
ZB25 1.6 N	37.5	2.3	11.6	30.5	116.4	35->59
ZB25 3.8 N	32.8	0.9	5.5	42.9	157.3	39->59
Zeolite Y						
CBV 500	21.7	0.2	0.1	24.7	111.5	50->75
CBV 600	20.5	0.2	0.2	28.4	122.7	51->81
CBV 712	25.1	0.5	0.6	32.4	130.4	34->69
CBV 720	26.3	0.8	1.4	32.7	129.6	34->64
CBV 740	27.5	0.5	2.7	33.5	132.9	44->69
CBV 760	29.0	0.9	4.3	35.4	136.6	49->69
CBV 780	25.2	0.5	3.6	32.5	130.6	34->64
ZSM-5						
CBV 3020	23.6	1.6	2.2	15.2	78.9	40->50
CBV 5020	26.7	2.1	4.2	26.3	108.2	40->55
CBV 8020	24.2	1.6	4.9	12.0	70.1	50->60
CBV 1502	24.0	0.2	n.d.	34.9	137.8	41->70
CBV 3002	16.3	0.3	n.d.	24.0	105.8	45->63
CBV 2802	19.7	0.4	n.d.	29.7	121.0	50->65
S.P. mordenites						
ZM 101	7.7	n.r.	n.r.	11.4	79.3	65->90
H3h	2.6	n.r.	n.r.	5.4	63.9	85->110
H24h	4.9	n.r.	n.r.	-3.0	36.0	85->103
550H550	17.5	0.6	0.5	4.6	52.9	60->79
600H600	15.6	0.6	1.3	5.4	55.0	55->80
S500 H	15.0	n.r.	n.r.	6.4	59.0	65->80
S600 H	15.8	0.2	1.2	7.4	61.1	50->80
S700 H	16.9	0.5	4.7	8.9	64.6	60->70
H24h S600 H	15.5	0.0	0.0	4.6	53.5	50->85
L.P. mordenites						
HSZ 600	11.6	0.1	0.1	18.2	94.8	55->80
H 9h	13.8	0.2	n.d.	9.1	68.6	70->80
S600 H1	20.6	0.9	2.0	2.0	44.0	60->75
550H550	17.2	0.6	2.8	3.2	48.5	60->82
700H700	15.4	0.4	2.8	7.1	60.5	61->81
S600 H	17.3	0.6	n.d.	7.7	63.1	71->81
S700 H	17.5	0.3	n.d.	8.3	64.6	61->81
H 24h S600 H	12.9	0.2	1.2	1.6	44.1	54->85
Zeolite omega						
LZ6	9.5	n.r.	n.r.	29.3	133.6	40->80
S700 H 0.24	14.0	0.0	n.d.	29.2	127.4	59->74
S600 H 0.24	15.5	0.1	n.d.	24.6	112.9	54->74
S650 H 0.24	15.3	0.1	n.d.	22.4	106.9	59->79
S600 H 1.22	16.9	0.1	0.1	23.6	109.4	59->74
S700 H 1.22	23.1	0.4	n.d.	18.8	92.4	59->74
S650 H 1.22	24.8	0.6	1.2	24.8	108.6	55->69
S675 H 1.22	25.6	0.5	1.0	32.9	131.3	55->65
S750 H 1.47	24.2	0.7	n.d.	32.0	128.7	55->69
S675 H 2.45	19.7	0.2	1.2	26.2	111.0	60->70
S750 H 1.22	26.0	0.4	1.2	22.4	102.7	60->74
Pillared clays						
Zr-P-M	28.6	0.1	n.d.	45.8	169.8	55->80
Al-P-S	19.4	0.0	n.d.	45.5	173.5	55->85
Resin						
Amberlyst-15	51.6	5.5	1.1	38.9	139.6	39->53

Note. The last column is the temperature range (in °C) where Ea app. and ln(ko app.) were calculated.

a, calculated by dividing the rate by the cation exchange capacity for beta, ZSM-5, modernites and Omega, by Al_{IV} (MAS-NMR) for zeolites Y and by 5 meq/g for Amberlyst-15.

pillared clays. For the reference resin, a value of 139 kJ/mol was found. Except for the beta zeolites, the sequence of the average activation energies is similar to that of the activities (reflected by the yields of MTBE at maximum conversion). Activation energies of 75 ± 10 kJ/mol and 135 kJ/mol were reported by Nikolopoulos *et al*. (21) in the temperature ranges of 60–90°C and 40–60°C, respectively. These authors suggested that the kinetic data obtained above 60°C could be partially influenced by internal diffusion. This interpretation may be invoked to explain the differences observed between the mordenites and the other zeolites. However, constraints imposed by the thermodynamics of the reaction may also be advocated, particularly for the less active mordenite catalysts. Besides, as the apparent activation energies include a contribution of the adsorption enthalpies, it is likely that this contribution will not be exactly the same at low and high temperature.

DISCUSSION

The discussion will be restricted to a few general features. A more elaborate discussion would evidently require a thorough characterization of the different zeolites tested (work in progress), which was out of the scope of these screening experiments. The most emerging result is certainly the high catalytic efficiency of the beta-type zeolites in the gas phase synthesis of MTBE with respect to the other zeolites. Indeed, comparable yields of the ether are produced over the most active sample of beta zeolite and Amberlyst-15, and even the least active samples of beta zeolite produce higher yields of MTBE than the most active ones among the different zeolites investigated.

A common feature shared by most of the zeolites considered is the enhancement of the catalytic activity upon dealumination, a behavior which has been observed in many proton-catalysed reactions in general, and in the reaction under investigation, in particular (15). It is usual to illustrate the effect of the Si/Al ratio by plots of conversion versus Si/Al ratio (or Al per unit cell). Such representations generally show an increase of the conversion up to a certain Si/Al ratio (depending, among others, on the type of zeolite) followed by a diminution of conversion as more framework Al atoms (hence, active sites) are removed. This general trend is partly found in our results. Indeed, the highest yields of MTBE were observed for zeolites with bulk Si/Al ratios between 13 and 35, namely: 21 for H-Y, 25 for H-ZSM-5, 13 for SP mordenites, 35 for LP mordenites, 26 for omega zeolite, and beta zeolite. This increase of activity with increasing Si/Al ratio has been accounted for by a reinforcement of the strength of the acid sites, which was corroborated from calculations based on topological Al density (34) and Monte Carlo simulations (35). This observation is valid, of course, as long as only the Al atoms which constitute the active sites (mainly framework Al IV) are taken into account in the Si/Al ratio. Solid-state MAS-NMR spectroscopy of ^{27}Al has clearly evidenced that Al with different environments (extraframework Al species) may result from dealumination treatments, in amounts and proportions which

depend, e.g., on the dealumination procedure and conditions and type of zeolite. It has not been possible to collect ^{27}Al NMR spectra for the different samples of the zeolites investigated. So far, only the H-Y series has been examined (36) and will be discussed below. Therefore, the Si/Al ratios at which maximum conversion of IB into MTBE is noticed are only indicative since they were established from bulk Al contents.

Several authors have shown, for different proton-catalyzed reactions, that beta zeolite was more active and selective (37–41), or more selective (38, 42–47) than other 12MR and 10MR zeolites. Only few authors, however, accounted for the higher performances of zeolite beta. Essentially the highly silicious nature of the interconnecting channels (39, 45), unique more open pore system allowing free access to the active sites (48), or highly active outer surface (49, 50) have been invoked as possible explanations. Borade *et al*. (51–52), from XPS measurements of the binding energy of the N1s peak of pyridine adsorbed over different 12MR acid zeolites, proposed the following sequence for the strength of the Brønsted acid sites: omega > beta ≥ H-ZSM-20 > mordenite > H-Y. Additional features, however, distinguish zeolite beta from other 12MR zeolites such as: extensive loss of framework Al upon calcination of NH_4-forms (53, 54), reversible transformation of framework Al^{IV} into framework Al^{VI} in the presence of water (55, 56), more complex acid function (54, 57–59). Considering the various particularities of beta zeolite, it may be that its catalytic behavior could be explained by a single feature. It may as well be that the explanation is more complex and involves several aspects, separately or in combination. Further characterization work is progressing in that direction.

In the gas phase synthesis of MTBE performed at 60°C over partially dealuminated H-Y zeolites (with Si/Al ratios of 6, 8, 14, and 18), Kogelbauer *et al*. (17) and Nikolopoulos *et al*. (18) observed a linear increase of the TOF (established from the initial rates) with decreasing acid site concentration (lattice Al). These authors suggested that this enhancement of the TOF was the result of mutual interaction between extra-lattice Al (presence confirmed by ^{27}Al MAS-NMR) and Brønsted acid sites, the lattice Al content being, indeed, too low as to exhibit "next nearest neighbor" effects (60, 61). The samples of zeolite H-Y tested in this study have been characterized by this spectroscopy and the proportions of the different Al species have been established (36). The values are reported in Table 3. The TOF were obtained from the rates measured at 60°C (Table 2) divided by the Alt (framework tetrahedral Al, NMR) content. The plot of the TOF versus Al^{IV}/unit cell is shown in Fig. 9. A nearly linear increase of the TOF as concentration of tetrahedral sites decreases is also observed for samples with bulk Si/Al ratios between 2.8 and 37. Now, if extraframework Al had a beneficial effect on the reaction, one would expect, as

TABLE 3

Concentrations (in meq/g) of Framework (Alt) (Signal at 60 ppm), Extraframework (Signal at 30 ppm) (Alx), Octahedral (Alo) (Signal at 0 ppm), and Invisible (Ali) Aluminium Species of Zeolite Y (Ref. (36)

Sample	Alt [a]	Alx [a]	Alo [a]	Alj [b]
CBV 500	1.643	1.205	1.157	0.620
CBV 600	0.878	0.668	0.99	1.846
CBV 712	0.750	0.189	0.746	0.782
CBV 720	0.613	0.058	0.062	0.455
CBV 740	0.201	0.037	0.084	0.435
CBV 760	0.217	0.008	0.076	0.236
CBV 780	0.132	0.034	0.050	0.223

a, from quantitative MAS-NMR.

b, calculated by subtracting the sum of Al obtained by quantitative MAS-NMR from total Al content (ICPS data).

it was observed in the case of heptane and decane isomerisation (36), an enhancement of the TOF with increasing content of extraframework Al(x) (Al species characterized by a NMR signal at 30 ppm attributed to pentacoordinated Al or distorted tetrahedral Al), or with Al(o) (octahedral extraframework Al species with NMR signal at 0 ppm). Against expectation, a drastic drop of the TOF with increasing Al(x) and Al(o) contents was obtained. A meaningful

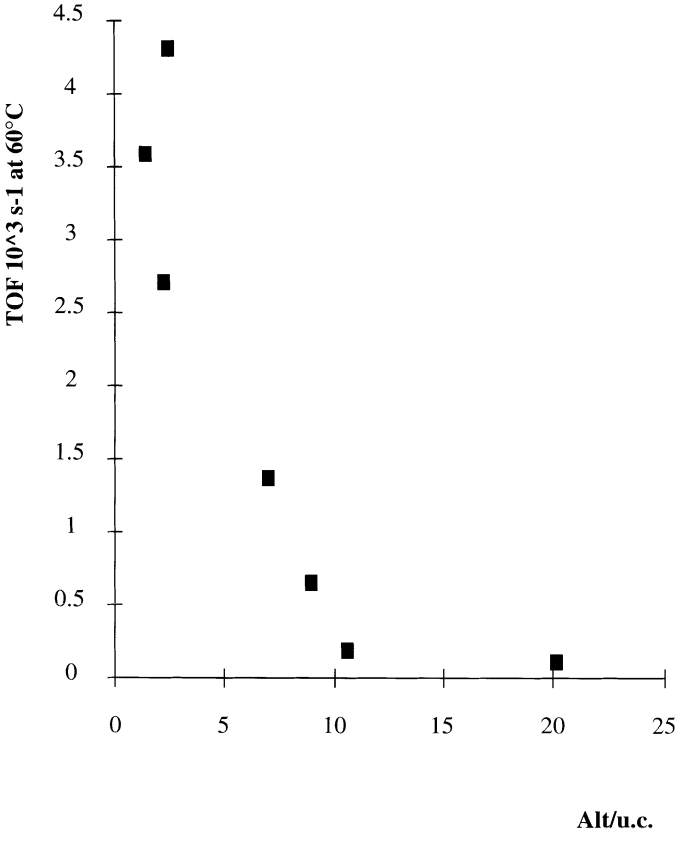

FIG. 9. Zeolites H-Y: Turnover frequency (10^3 s^{-1}) at 60°C vs Al(t) (tetrahedral aluminium) per unit cell.

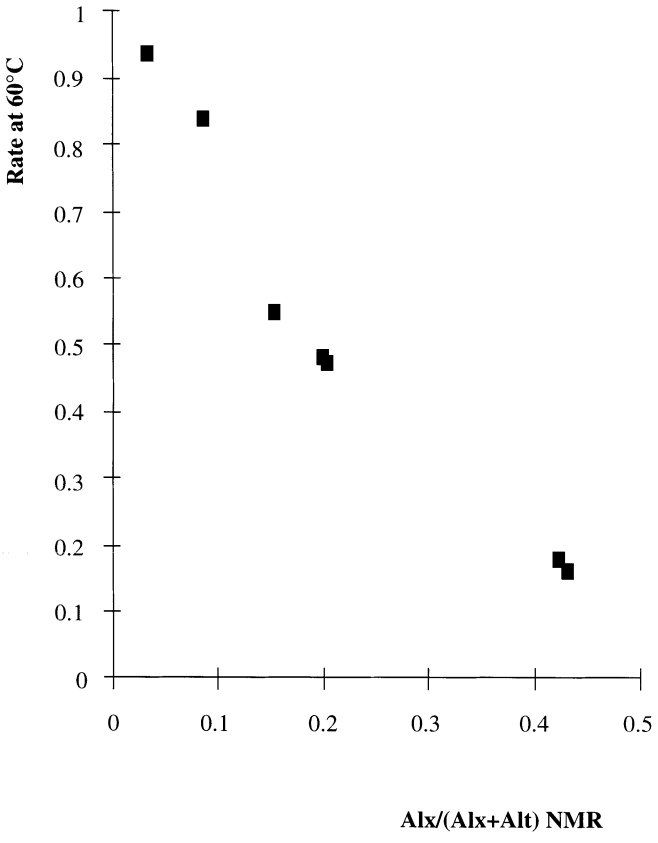

FIG. 10. Zeolites H-Y: Reaction rate at 60°C (in mmol g^{-1} s^{-1}) vs Alx/(Alx + Alt) ratio (Alx: extraframework Al with NMR signal at 30 ppm; Alt: lattice Al with NMR signal at 60 ppm).

relationship could be found between the reaction rates (at 60°C) and the relative amount of Al(x), as illustrated in Fig. 10. The unfavorable influence of Al(x) (extraframework Al^{V} or distorded framework Al^{IV}) on the reaction rate is obvious. Kogelbauer *et al.* (18) and Nikolopoulos *et al.* (21) found that the TOF increased almost linearly with the extralattice/lattice Al ratio. These authors suggested that the positive influence of extralattice Al could be due to an enhancement of the acid strength of the sites associated with lattice Al by a possible coupling with neighboring strong Lewis sites associated with extralattice Al (the nature of this latter species being not clear). Our data did not provide a similar relationship. Instead, plotting the TOF values versus the Al(o)/Al(t) ratios showed an inverse effect, namely a decrease of TOF with increasing ratios (except for sample CBV 720). No convincing relation (high scattering) could be found between TOFs and Al(x)/Al(t) ratios. The disagreement with the observations of Kogelbauer *et al.* (18) and Nikolopoulos *et al.* (21) is not yet understood and further investigation is necessary to explain it.

Similar relationships could not be established for the other zeolites as the distributions of the different Al species have not yet been established. The TOF values given in Table 2 were obtained from the CEC data (microkjeldahl analyses) of samples exchanged with 1 M ammonium acetate, assuming that only tetrahedral Al positions were occupied by ammonium. They may only have a limited value since the Al^{IV} contents have not been controlled by a more direct method.

Contribution of the External Surface Area to the Reaction

As outlined earlier, the beta zeolites have substantially higher external surface areas compared with the values found for the other series of dealuminated zeolites (see Table 1). For the reason invoked above, the Sext have not been determined for the series of omega zeolites.

If the external surface (Sext) was involved, at least partly, in the overall reaction, one would expect some relationship between this parameter and a measure of the activity. In Fig. 11, the yields of MTBE at maximum conversion obtained for the series of beta, Y, ZSM-5, and mordenites have been plotted against the external surface areas (Sext). Despite some scattering of the experimental values, there seems to be, indeed, a link between these two parameters. A similar trend was observed between the rate at 60°C and Sext. It was also verified that no coherent variation existed when the micropore volumes were used instead of the external areas. The average micropore volumes determined from nitrogen sorption isotherms were as follows: 0.268 cm^3/g for the H-Y samples; 0.214 cm^3/g for the series of beta zeolites; 0.193 cm^3/g for the SP modenites, 0.201 cm^3/g for the LP mordenites and 0.134 cm^3/g for H-ZSM-5, thus, in a different sequence than for the activities. Thus, the acidity of the external surface appears to contribute to the catalytic activity of the different zeolites. In the study over the series of H-Y mentioned above (36), it was shown by XPS that the outer surface of samples CBV-500, -600, and -712 was enriched in Al (migration of Al toward the periphery of the crystallites during the steaming treatment) whereas for CBV-720, -740 , -760, and -780 (acid leached after steaming), the outer surface was depleted in Al with respect to the bulk Al content (established by ICP analysis and MAS-NMR). Monitoring the acidity at the outer surface by ammonia adsorption, surface N/Al ratios were established. Values between 0.05 and 0.25 were obtained for the steamed samples (CBV-500, -600, -712, the least active ones among the series), and between 0.80 and 0.99 for the steamed and acid leached samples (CBV-720 to -760, the most active ones), thus indicating that the majority of the extra-lattice Al at the Al-enriched outer surface is nonacidic in the first series and that in the second series the Al-depleted outer surface (resulting from the removal of these species by the subsequent acid leaching) is relatively more acidic (less acid sites but sites with higher strengths and/or sites unoccupied by extraframework species).

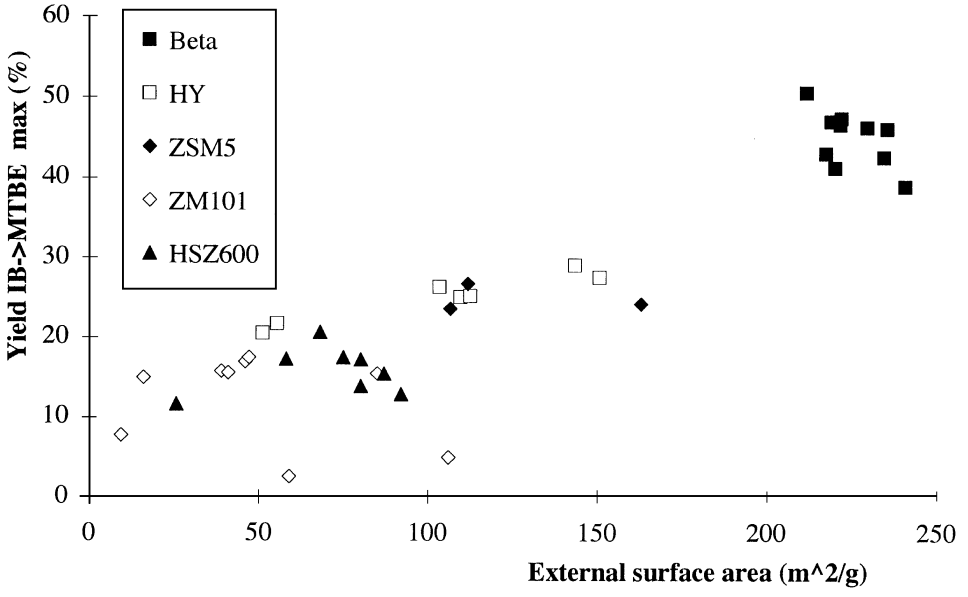

FIG. 11. Yield of MTBE at maximum conversion vs external surface area (Sext) of the zeolites.

Compensation Effect

Figure 12 shows the relation between the activation energy and logarithm of the preexponential term of Arrhenius' equation. In the literature, a relation of the type $Ea = a + b \ln k$ is indicative of compensation (isokinetic) effect. In Fig. 12, the values of the constants are: $a = 42.8$ and $b = 2.65$. They are coherent with those compiled by Corma *et al.* (62) from literature data concerning different acid–base catalyzed reactions performed over zeolites. These authors interpreted this effect as a consequence of the changes of the acidity of the active sites brought about

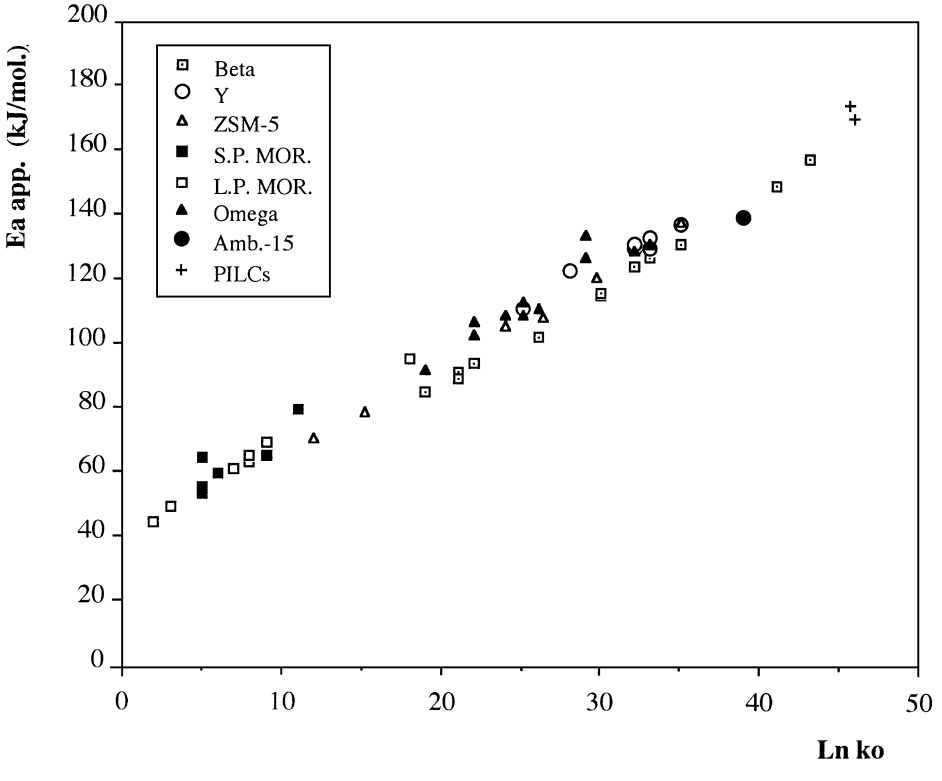

FIG. 12. Apparent activation energy (Ea app) vs ln ko for the different zeolites.

by (partial) cation exchange and (as in the present study) by modifying the Si/Al ratio. Different causes have been suggested to explain the CE (see References in (63)), the most convincing one being the approach based on changes in the energy levels of the transition state, proposed by Conner (60) and modified by Patterson and Rooney (64).

CONCLUSION

Gas phase synthesis of methyl-tertio butyl ether performed over different dealuminated acid zeolites and pillared clays has shown the following sequence in activity: beta zeolite = Amb.-15 (ref.) > H-Y = Zr-PILC > omega ≥ H-ZSM-5 > LP MOR > SP MOR > Al-PILC > SAPOs. Dealumination has a beneficial effect on the reaction, the highest conversions being reached for bulk Si/Al ratios between 13 and 35, according to the type of zeolite. The external surface area appears to contribute to the reaction: beta zeolite, the most active one, also has the greater Sext value. As discussed for the series of H-Y zeolites, extraframework Al species (both in surface and bulk), have a detrimental influence on the reaction.

ACKNOWLEDGMENT

F. Collignon gratefully acknowledges F.R.I.A., Belgium, for a doctoral grant.

REFERENCES

1. Hälsig, C. P., Gregory, P., and Peacock, T., *Spec. Publ. R. Soc. Chem.* **97**, 311 (1991).
2. Peaff, G., *Chem. Eng. News* **8** (1994).
3. Chaumette, S., and Torck, B., *Rev. Inst. Français Pétrole* **49**(6), 641 (1994).
4. Lee, A. K. K., and Al-Jarallah, A., *Chem. Econ. Eng. Rev.* **18**(9), 25 (1986).
5. Vila, M., Cunill, F., Izquierdo, J. P., Gonzalez, J., and Hernandez, A., *Appl. Catal.* **117**, L99 (1994).
6. Vincencio, G. T., Ramos, A. O., Villanveva, J. R., and Lopez, G. P., *Rev. Inst. Mexicano Petrol.* **14**, 66 (1987).
7. Shikata, S., Okuhara, T., and Misono, M., *J. Mol. Catal.* **100**, 49 (1995).
8. Yadav, G. D., and Kirthivasan, N., *J. Chem. Soc. Chem. Commun.* **203** (1995).
9. Cheng, S., Wang, J.-T., and Lin, C.-L., *J. Chin. Chem. Soc.* **38**, 529 (1991).
10. Feeley, O. C., Johansson, M. A., Herman, R. G., and Klier, K., *Prep. Pap. Am. Chem. Soc. Fuel Chem.* **37**(4), 1817 (1992).
11. Ushikubo, T., and Wada, K., *Appl. Catal.* **124**, 19 (1995).
12. Nicolaides, C. P., Stotijn, C. J., van der Veen, E. R. A., and Visser, M. S., *Appl. Catal.* **103**, 223 (1993).
13. Larsen, G., Lotero, E., Marquez, M., and Silva, H., *J. Catal.* **157**, 645 (1995).
14. Chu, P., and Kühl, G. H., *Ind. Chem. Res.* **26**, 365 (1987).
15. Nikolopoulos, A. A., Oukaci, R., Goodwin Jr., J. G., and Marcelin, G., *Catal. Lett.* **27**, 149 (1994).
16. Chang, K.-H., Kim, G.-J., and Ahn, W.-S., *Ind. Eng. Chem. Res.* **31**, 125 (1992).
17. Kogelbauer, A., Nikolopoulos, A. A., Goodwin Jr., J. G., and Marcelin, G., *in* "Studies in Surface Science and Catalysis," Vol. 84, p. 1685, Elsevier Sci., Amsterdam, 1994.
18. Nikolopoulos, A. A., Kogelbauer, A., Goodwin Jr., J. G., and Marcelin, G., *Appl. Catal.* **119**, 69 (1994).
19. Le Van Mao, R., Carli, R., Ahlafi, H., and Ragaini, V., *Catal. Lett.* **6**, 321 (1990).
20. Nikolopoulos, A. A., Kogelbauer, A., Goodwin Jr., J. G., and Marcelin, G., *J. Catal.* **158**, 76 (1996).
21. Nikolopoulos, A.A., Kogelbauer, A., Goodwin Jr., J.G., and Marcelin, G., *Catal. Lett.* **39**, 173 (1996).
22. Rodriguez-Ramos, I., Guerrero-Ruiz, A., and Fierro, J. L. C., *Prep. Div. Petr. Chem.* **36**(4), 804 (1990).
23. Kogelbauer, A., Ocal, M., Nikolopoulos, A. A., Goodwin Jr., J. G., and Marcelin, G., *J. Catal.* **148**, 157 (1994).
24. Kogelbauer, A., Nikolopoulos, A. A., Goodwin Jr., J. G., and Marcelin, G., *J. Catal.* **152**, 122 (1995).
25. Moreno, S., and Poncelet, G., submitted.
26. Fajula, F., Bourgeat-Lami, E., Zivkov, C., Des Courières, T., and Anglerot, D., Fr. Pat. 2,069,618 (1992).
27. Jaquinot, E., Raatz, F., Macedo, A., and Marcilly, C., *in* "Studies in Surface Science and Catalysis," Vol. 46, p. 118, Elsevier Sci., Amsterdem, 1989.
28. Ponthieu, E., Grange, P., Joly, J.-F., and Raatz, F., *Zeolites* **12**, 395 (1992).
29. Moreno, S., Sun Kou, R., and Poncelet, G., *J. Catal.* **162**, 198 (1996).
30. Moreno, S., Sun Kou, R., and Poncelet, G., *J. Phys. Chem.*, in press.
31. Voloch, M., Ladisch, M. R., and Tsao, G. T., *React. Polymers* **4**, 9 (1986).
32. Remy, M. J., and Poncelet, G., *J. Phys. Chem.* **99**, 773 (1995).
33. Tejero, J., Cunill, F., and Izquierdo, J. F., *Ind. Eng. Chem. Res.* **27**, 338 (1988).
34. Barthomeuf, D., *in* "Studies in Surface Science and Catalysis," Vol. 33, p. 177, Elsevier Sci., Amsterdam, 1987.
35. Ding, T. D., Sun, P. C., Jin, Q. H., Li, B. H., and Wang, J. Z., *Zeolites* **14**, 61 (1994).
36. Remy, M. J., Stanica, D., Poncelet, G., Feijen, E. J. P., Grobet, P. J., Martens, J. A., and Jacobs, P. A., *J. Phys. Chem.* **100**, 12440 (1996).
37. Bandyopadhyay, R., Singh, P. S., and Shaikh, R. A., *Appl. Catal.* **135**, 249 (1996).
38. Chu, S.-J., and Chen, Y.-W., *Appl. Catal.* **123**, 51 (1995).
39. Reddy, K. S. N., Rao, B. S., and Shiralkar, V. P., *Appl. Catal.* **121**, 191 (1995).
40. Bellussi, G., Pazzuconi, G., Perego, C., Girotti, G., and Terzoni, G., *J. Catal.* **157**, 227 (1995).
41. Das, J., Bhat, Y. S., Bhardwaj, A. I., and Halgeri, A. B., *Appl. Catal.* **116**, 71 (1994).
42. Climent, M. J., Corma, A., Garcia, H., Iborra, S., and Primo, J., *Appl. Catal.* **130**, 5 (1995).
43. Shen, J.-P., Ma, J., Jiang, D.-Z., and Min, E.-Z., *Catal. Lett.* **26**, 291 (1994).
44. Hutchings, G. J., Johnston, P., Lee, D. F., and Williams, C. D., *Catal. Lett.* **21**, 49 (1993).
45. Reddy, K. S. N., Rao, B. S., and Shiralkar, V. P., *Appl. Catal.* **95**, 53 (1993).
46. Tsai, T.-C., Ay, C.-L., and Wang, I., *Appl. Catal.* **77**, 199 (1991).
47. Corma, A., Gomez, V., and Martinez, A., *Appl. Catal.* **119**, 83 (1994).
48. Briscoe, N. A., Gasci, J. L., Daniels, J. A., Johnson, D. W., Shannon, M. D., and Stewart, A., *in* "Studies in Surface Science and Catalysis," Vol. 49, p. 151, Elsevier Sci., Amsterdam, 1989.
49. Elings, J. A., Downing, R. S., and Sheldon, R. A., *in* "Studies in Surface Science and Catalysis," Vol. 94, p. 487, Elsevier Sci., Amsterdam, 1995.
50. Harvey, G., Binder, G., and Prins, R., *in* "Studies in Surface Science and Catalysis," Vol. 94, p. 3978, Elsevier Sci., Amsterdam, 1995.
51. Borade, R. B., and Clearfield, A., *in* "Studies in Surface Science and Catalysis," Vol. 84, p. 661, Elsevier Sci., Amsterdam, 1994.
52. Borade, R. B., and Clearfield, A., *J. Phys. Chem.* **96**, 6729 (1992).
53. Bourgeat-Lami, E., Massiani, P., Di Renzo, F., Fajula, F., and Des Courières, T., *Catal. Lett.* **5**, 265 (1990).

54. Kiricsi, I., Flego, C., Pazzuconi, G., Parker Jr., W. O., Millini, R., Perego, C., and Bellussi, G., *J. Phys. Chem*. **98**, 4627 (1994).
55. Bourgeat-Lami, E., Massiani, P., Di Renzo, F., Espiau, P., and Fajula, F., *Appl. Catal.* **72**, 139 (1991).
56. de Ménorval, L. C., Buckermann, W., Figueras, F., and Fajula, F., *J. Phys. Chem*. **100**, 465 (1996).
57. Beck, L. W., and Haw, J. F., *J. Phys. Chem*. **99**, 1076 (1996).
58. Jia, C., Massiani, P., and Barthomeuf, D., *J. Chem. Soc. Faraday Trans.* **89**(19), 3659 (1993).
59. Maache, M., Janin, A., Lavalley, J. C., Joly, J.-F., and Benazzi, E., *Zeolites* **13**, 419 (1993).
60. DeCanio, S. J., Sohn, J. R., and Lunsford, J. H., *J. Catal.* **101**, 132 (1986).
61. Shertukde, P. V., Marcelin, G., Sill, G. A., and Hall, K. W., *J. Catal.* **136**, 446 (1992).
62. Corma, A., Llopis, F., Monton, J. B., and Weller, S., *J. Catal.* **142**, 97 (1993).
63. Conner, W. C., *J. Catal.* **78**, 238 (1982).
64. Patterson, W. R., and Rooney, J. J., *J. Catal.* **146**, 310 (1994).